American Journal of Modern Energy
2023; 9(4): 77-83
http://www.sciencepublishinggroup.com/j/ajme
doi: 10.11648/j.ajme.20230904.11
ISSN: 2575-3908 (Print); ISSN: 2575-3797 (Online)

Numerical Modelling and Analysis of Photovoltaic-Thermal Liquid Collector Using OpenFOAM

Ashutosh Dev*, Bikram Singh Bhattarai

Department of Mechanical Engineering, Kathmandu University, Dhulikhel, Nepal

Email address:
Devashutosh31@gmail.com (Ashutosh Dev)

*Corresponding author

To cite this article:
Ashutosh Dev, Bikram Singh Bhattarai. (2023). Numerical Modelling and Analysis of Photovoltaic-Thermal Liquid Collector using OpenFOAM. *American Journal of Modern Energy*, *9*(4), 77-83. https://doi.org/10.11648/j.ajme.20230904.11

Received: August 26, 2023; **Accepted**: September 13, 2023; **Published**: December 28, 2023

Abstract: This paper presents a comprehensive study on the performance of a solar photovoltaic-thermal (PVT) system with a single water pipe as the working fluid. The investigation focuses on mathematical modeling using the OpenFOAMv9 software package and visualization through Paraview. The primary objective is to evaluate the thermal and electrical efficiency of the PVT collector while analyzing its transient response. In this research, steady-state and transient analyses of the solar PVT system are conducted under various water mass flow rates and solar radiation levels, employing the chtMultiRegionFoam solver. The study includes the variation of water outlet temperature concerning mass flow rates for solar radiations at 700 W/m² and 1000 W/m². Simulation results closely align with analytically calculated thermal efficiencies by Chow T., demonstrating the validity of the approach. Thermal efficiency remains consistent between the two radiation levels. The analysis reveals that the electrical efficiency is superior at 700 W/m² due to reduced heating and lower silicon cell temperatures. Moreover, both thermal and electrical efficiencies exhibit an increasing trend with higher water mass flow rates. The study also presents the transient response of the PVT system when reducing the mass flow rate from 0.002 kg/s to 0.001 kg/s. The successful simulation of this PVT system classifies the employed CFD package as capable and effective. This research contributes to a deeper understanding of PVT system performance and offers insights into enhancing its efficiency under various operational conditions. The findings hold significance for the design and optimization of solar PVT systems to harness both thermal and electrical energy effectively. Additionally, the research highlights the utilization of the OpenFOAM platform for simulating this specific case.

Keywords: Solar Photovoltaic-Thermal System, Thermal Collector, OpenFOAM, Mathematical Modeling, Transient Response

1. Introduction

The Photovoltaic thermal liquid collector serves as a pivotal solution for converting solar energy. This technology combines solar thermal and solar photovoltaic conversion methods, enabling the simultaneous generation of electricity and heat from solar radiation. This dual approach not only produces usable power but also effectively harnesses solar energy to generate both electricity and heat concurrently, thereby maximizing the overall benefits of solar radiation utilization. This temperature rises stems from the interactions involving photonic particles. The heightened temperature has a negative impact on the mobility of electrons, causing the recombination of electron-hole pairs. As a consequence, the electrical efficiency experiences a decline [1]. In light of existing literature, a comprehensive study was undertaken to examine the effectiveness of efficiencies and transient response in the context of Nepal's climatic conditions [2].

The backdrop for this investigation arises from the pressing issues of elevated electricity consumption, steep operational expenses, and the detrimental ecological impact associated with conventional electricity sources. In response, scholars have initiated endeavors centered around power generation systems and solar photovoltaic technology, aiming to enhance the capacity for electricity generation through renewable energy means [3]. Indeed, a comparative study was conducted, focusing on three unique configurations of hybrid PVT (Photovoltaic-Thermal) air solar collectors. These configurations included unglazed

hybrid photovoltaic thermal tiles, glazed hybrid photovoltaic thermal tiles, and conventional hybrid photovoltaic thermal air collectors. The research entailed a theoretical evaluation of four different arrangements of the optical-thermal air collector [4]. Further, distinct refrigerated PV (Photovoltaic) cells were utilized, and the thermal absorption configurations were positioned at the rear of the cell. Through a consideration of varying water flow rates, a spiral design operating at 0.01 kg/s was validated as the optimal configuration, yielding the highest combined thermal and electrical efficiency at 50.12% and 11.98%, respectively [5]. The operational and thermal performance of the PVT system employing a water tube was subjected to numerical analysis. This examination encompassed three distinct absorber types, culminating in a peak thermal efficiency of 66.8% and an electrical efficiency of 12.1%, notably achieved by the PV module featuring an absorber covering 50% of its surface.

Teo et al. [6] undertook the design and examination of a hybrid PVT solar system. Within this setup, PV cells received active cooling through a parallel arrangement of ducts, facilitated by inlet and outlet manifolds ensuring consistent airflow. A comparison was drawn between the efficiency of uncooled PV modules and those subjected to cooling. Uncooled PV modules demonstrated efficiencies spanning 8% to 9%, whereas active cooling elevated solar cell efficiencies to a range of 12% to 14%. On a daily average, thermal and electrical efficiencies reached approximately 50.5% and 10.5%, respectively [7]. The findings illuminated that electrical efficiency escalates with higher wind speeds but diminishes with increased spacing between the tubes. Conversely, thermal efficiency thrives when wind speed and tube spacing decrease. Investigating the interplay of optical and meteorological factors on heat transfer in a PVT water system across diverse geometric cooling system configurations, a numerical exploration was conducted [8]. Over the past decade, multiple studies have been executed to refine the efficacy of these systems and gauge their economic and environmental aspects [9]. An examination was carried out with the aim of exploring a glazed photovoltaic thermal air PVT (Photovoltaic-Thermal) system, both in the context of single and double-pass air heaters, catering to space heating and drying objectives. In pursuit of this, distinct thermal models were formulated for each of the systems [10]. The outcomes of the investigation highlighted an increase in thermal energy output for the glazed PVT system, driven by relatively lower electrical efficiency attributed to elevated operating temperatures. Furthermore, an investigation was conducted into the performance of a concentrating photovoltaic thermal solar collector. The analysis concluded that such systems demonstrated an overall thermal efficiency of 58% and an electrical efficiency of 11%, contributing to an aggregate system efficiency of 69% [11].

In previous research and the information mentioned earlier, there's a lack of detailed studies that look at solar systems with a mix of sunlight and water flow at different rates. Addressing this research gap, our study presents an innovative solution. Through our research paper, we examine the interplay between water mass flow rates, solar irradiation levels, and the performance of solar PVT systems. We showcase the correlation between water outlet temperature and diverse mass flow rates across varying solar irradiation scenarios. Our investigation notably unfolds the thermal efficiency under different irradiation levels, aligning our findings with established benchmarks such as Chow T's calculations. Additionally, we present transient response of the PVT system as mass flow rates are deliberately reduced. In essence, our research paper encapsulates a comprehensive exploration, shedding light on nuanced system behaviors and offering valuable insights into the optimization of solar PVT systems. This study focuses on a specific part of a solar PVT system that includes a single water pipe. We used mathematical modeling tools provided by the OpenFOAMv7 software [12] to understand how this system works. To make sense of the data we got from the modeling, we used another tool called Paraview [13]. This study utilized the chtMultiRegionFoam solver, an integral part of OpenFOAM software. This solver specializes in simulating heat transfer across various regions, enabling us to model the interplay of temperature and fluid flow within the solar PVT system. Through this tool, we gained insights into the system's behavior and the relationships between its components [12].

2. Mathematical Modeling

2.1. Problem Statement

This study uses a specific segment of a solar PVT system, centered around a single water pipe. Illustrated in Figure 1, the provided diagram delves into geometry and dimensions. As illustrated in Figure 1, the initial node labeled as 'g' pertains to the glass cover. The subsequent node denoted as 'p' corresponds to the PV plate. Following that, the 'b' node designates the thin-plate absorber. Moving along, the 't' node signifies the metallic bond between the plate and the tube, while the 'i' node is allocated for the insulation layer. Additionally, the 'w1' node designates the water within the tube.

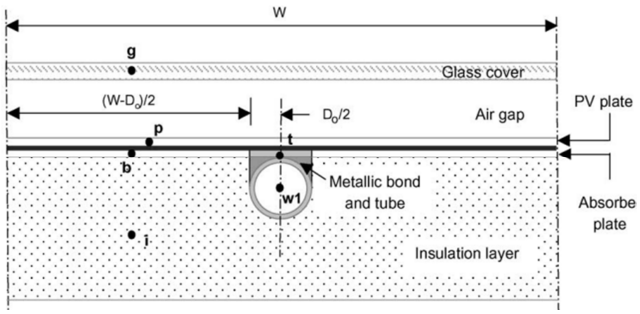

Figure 1. *Computational Domain Section.*

In our simulation, we adopt the parameters outlined by Chow T [5]. This includes investigating water flow rates ranging from 0 to 0.016 kg/s, spanning two solar radiation levels (700 W/m² and 1000 W/m²). [5] The determination of heat transfer coefficients employs specific formulas: h = 5.7 + 3.8v for glass surfaces and h = 2.8 + 3.8v for other surfaces [5]. The geometry, extending over a length of 1.6 m, follows

the parameter values extracted from Chow T's paper. To validate our simulation outcomes, we will utilize parameters similar to those used in Chow T's study and compare our model's results with Chow T's finding [5].

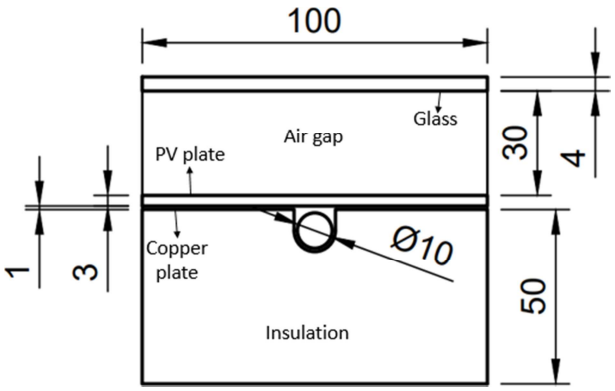

Figure 2. *Computational Geometry.*

2.2. Governing Equations

The governing equations employed in this study encompass continuity, momentum, and energy conservation equations, establishing a connection between fluid and solid behaviors. To depict turbulent flow characteristics, the k-ε model is utilized. The suitable conditions were applied on computational domain as per physics of the problem.

2.2.1. Continuity Equation

Continuity equation for incompressible fluid is defined as:

$$\frac{\partial u_i}{\partial x_i} = 0 \tag{1}$$

2.2.2. Momentum Equation

Momentum equation for incompressible fluid is defined as:

$$\frac{\partial(\rho u_i)}{\partial t} + \frac{\partial(\rho u_i u_j)}{\partial x_j} = \frac{\partial p}{\partial x_j} + \mu \frac{\partial^2 u_i}{\partial x_j \partial x_j} + \rho g_i \tag{2}$$

Where u is velocity, ρ is density of the fluid, p is pressure and gi is gravity, μ is viscosity.

2.2.3. Energy Conservation in Fluid

$$\frac{D}{Dt}\left(\rho\left(e + \frac{1}{2i}u^2\right)\right) = \frac{\partial q_i}{\partial x_i} + \frac{\partial^2 \tau_{ij} u_i}{\partial x_j} + \rho g_i u_i + S \tag{3}$$

Where e is internal energy, τ_{ij} is viscous stress, q_i is heat transferred by diffusion, S is heat source term.

2.2.4. Energy Conservation in Solid

$$\frac{\partial(\rho e)}{\partial t} = \frac{\partial}{\partial x_j}\left(\alpha \frac{\partial e}{\partial x_j}\right) \tag{4}$$

Where e is internal energy and α is thermal diffusivity

2.2.5. Coupling Between Fluid and Solid

Temperature of both fluid and solid is same at the interface.

$$Tf = Ts \tag{5}$$

Heat flux is same for both fluid and solid at the interface.

$$Q_f = -Q_s \tag{6}$$

$$k_f \frac{dT_f}{dn} = -k_s \frac{dT_s}{dn} \tag{7}$$

Where n is normal direction to the wall, k_f and k_s are thermal conductivity of fluid and solid.

3. Simulation Procedure

3.1. Geometry and Mesh

Due to the complexity of the system, a decision was made to implement a 2D model instead of a full 3D representation. This choice was driven by the need to save computational time while still capturing the essential characteristics of the problem. This pragmatic approach allows us to balance computational efficiency with accurate representation, enhancing the reliability of our simulation results.

The mesh for this study was generated using the blockMesh utility within OpenFOAM. A structured mesh approach was chosen, ensuring orderly divisions. Figure 3 illustrates the mesh configuration, which expands into the third dimension to fully represent the computational domain. Notably, the mesh is strategically refined in proximity to the water pipe to enhance the precision of our results. To achieve this, distinct cell sets are defined in the blockMeshDict file, catering to various regions within the domain. These cell sets are subsequently segmented into separate regions using the splitMeshRegions function. This mesh design aims to capture the nuances of the system, contributing to the accuracy and reliability of the simulation outcomes [14].

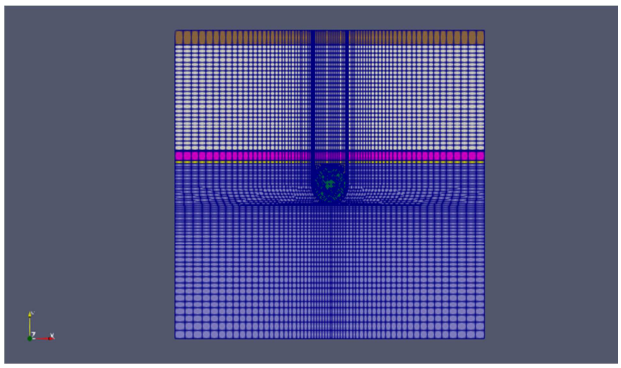

Figure 3. *Computational mesh.*

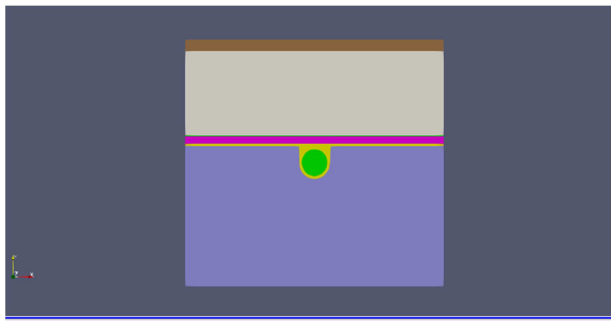

Figure 4. *2D Computational domain.*

3.2. Grid Independence Study

Grid independence study is done to find minimum number of cells for which results of the simulation does not depend on mesh size. For structured meshes with 63600, 208200, 468480, 880800 cells were considered four grid independence study. Average water outlet temperature for these four meshes is given in table 1. Temperature change is not significant between mesh 3 and mesh 4. So other simulations were done on settings based in mesh 3.

Table 1. *Grid Independence Study.*

Mesh Parameter (Cells)	Water Outlet Temperature (K)
63600	312.78
208200	309.86
468480	308.59
880800	308.55

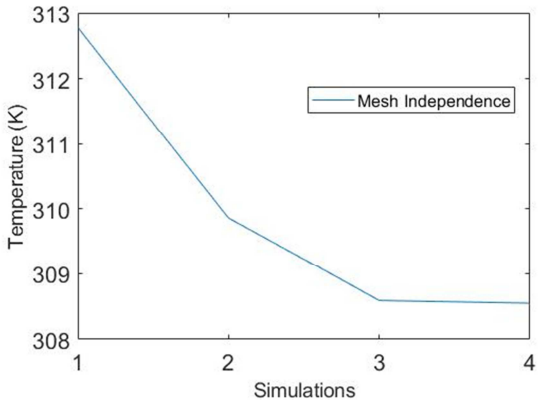

Figure 5. *Mesh Independency Test.*

3.3. Initial and Boundary Conditions

Boundary conditions for fluid:

Table 2. *Boundary conditions for fluid.*

Boundry	P_rgh	U	T
Inlet	fixedFluxPressure	fixedValue – uniform 0.025	fixedValue – uniform 300
Outlet	fixedValue – uniform 0	pressureInletOutletVelocity	inletOutlet
Wall	fixedFluxPressure	noSlip	compressible: turbulent TemperatureCoupledBaffle Mixed

Boundary condition for solid:

Table 3. *Boundary conditions for solid.*

Boundary	T
Side walls	zeroGradient
Front and back wall	externalWallHeatFluxTemperature
Top wall	externalWallHeatFluxTemperature
Bottom wall	externalWallHeatFluxTemperature

For all interfaces between two materials, compressible: turbulent Temperature Coupled Baffle Mixed boundary condition is used. At t = 0, velocity is uniform 0, pressure is uniform 0 and temperature is uniform 300.

3.4. Solver

chtMultiRegionFoam is used for this problem due to heat transfer between multiple regions. It is a transient solver for fluid flow and solid heat conduction with conjugate heat transfer between solid and fluid regions with buoyancy effect, turbulence, reaction and radiation modelling. The solver employs a segregated solution strategy, where the equations corresponding to each individual variable within the system are addressed sequentially. This involves solving the equations one after the other, with the solution from earlier equations being integrated into subsequent ones [15].

This approach is also extended to the interaction between the fluid and solid components. Initially, the fluid equations are tackled, utilizing the solid temperature from the previous iteration to establish boundary conditions for the fluid temperature. Subsequently, the solid equations are solved, leveraging the fluid temperature from the previous iteration to define boundary conditions for the solid temperature. This iterative process continues until a state of convergence is reached, signifying that the solutions have stabilized [15].

3.5. Post-Processing

Average water outlet temperature is calculated by following formula [16]:

$$T = \frac{2}{V_m R^2} \int_0^R T(r)V(r)\,dr \tag{8}$$

Thermal efficiency of the PVT system can be calculated by following formula:

$$\eta t = \frac{\dot{m} C_p (T_o - T_i)}{A \times G} \tag{9}$$

Where η_{th} is thermal efficiency, $\dot{m}$ is mass flow rate, C_p is heat capacity of water, T_o and T_i are water outlet and inlet temperature, A is area of the collector, G is solar irradiance [5].

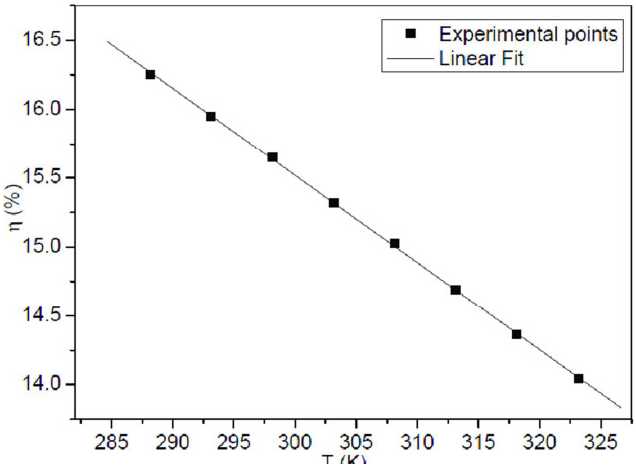

Figure 6. *Electrical Efficiency [17].*

Electrical efficiency of the silicon cell is determined from temperature of the silicon cell using following graph [17].

4. Results and Discussion

Illustrated in Figure 7 is a plot depicting the modulation of water outlet temperature in response to diverse mass flow rates, encompassing solar radiation levels of both 700 W/m² and 1000 W/m². Progressing to Figure 8, we see examination of thermal efficiency fluctuations under a solar radiation intensity of 1000 W/m², concurrently affirming the precision of these efficiency measures. A salient observation materializes at this juncture: the thermal efficiencies attained through OpenFOAM simulation exhibit a close alignment with the values computed by Chow T [5]. This remarkable congruence between the simulation results and the analytical data by Chow T validates the accuracy and reliability of the conducted simulation.

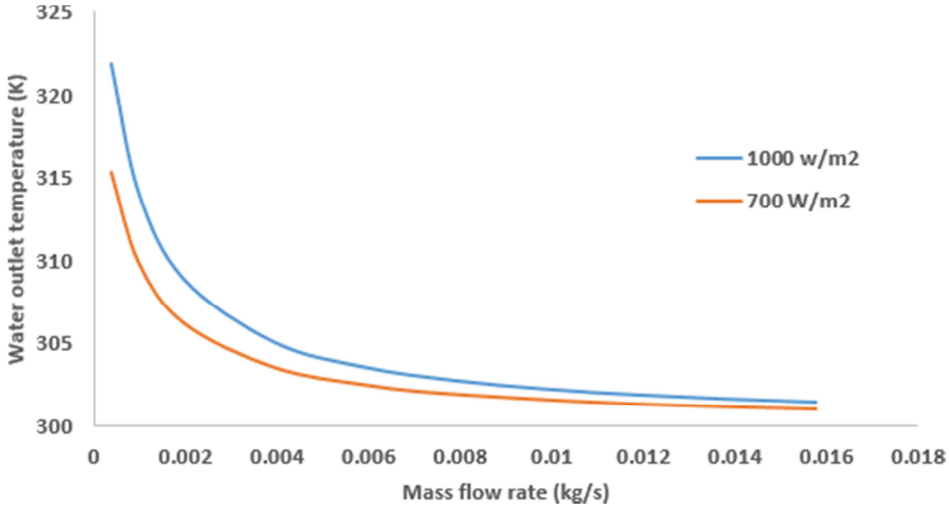

Figure 7. *Water outlet temperature.*

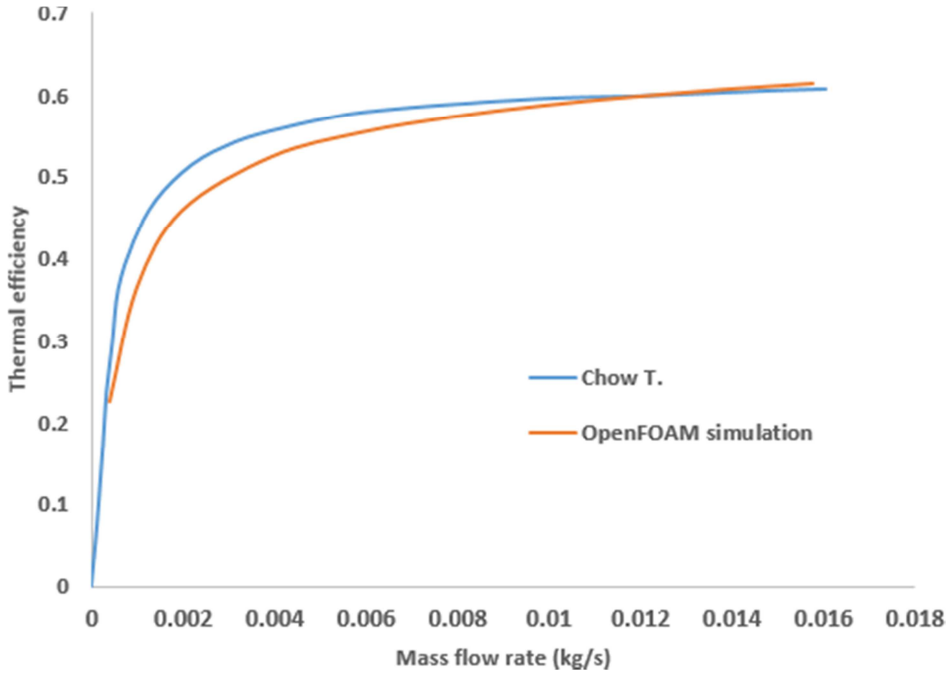

Figure 8. *Thermal efficiency for 1000 W/m².*

Shifting focus to Figure 9, we examine the variation in thermal efficiency at a constant solar radiation level of 700 W/m². Surprisingly, the thermal efficiency remains consistent across both 700 W/m² and 1000 W/m² radiation levels. Figure 10, takes us through the transformation of electrical efficiency at 700 W/m² and 1000 W/m². Here, the higher electrical efficiency observed at 700 W/m² is attributed to reduced heat generation and the subsequent lower temperature of the silicon cell. These visualizations collectively provide a comprehensive understanding of how the system responds to different scenarios, reaffirming the reliability of our simulation results and their alignment with practical observations.

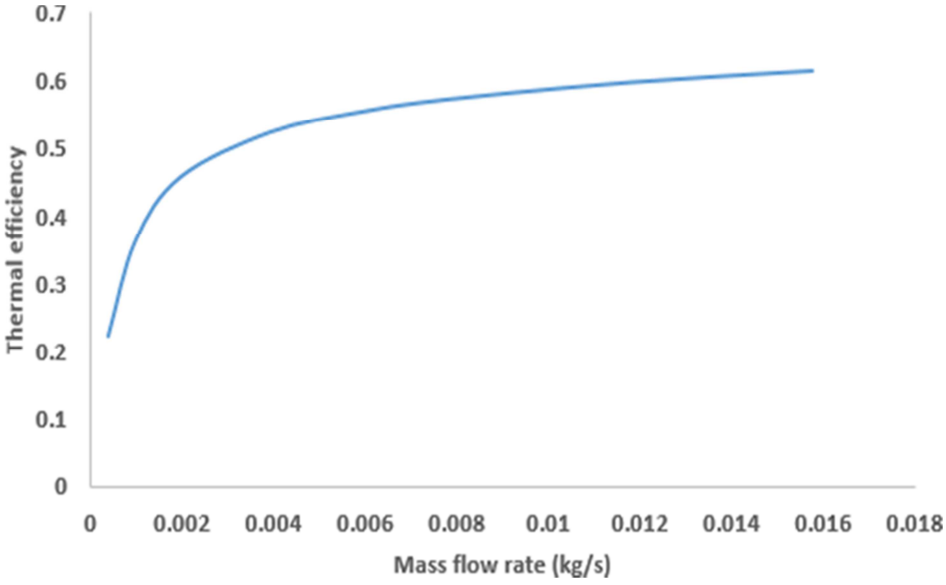

Figure 9. *Thermal efficiency for 700 W/m^2.*

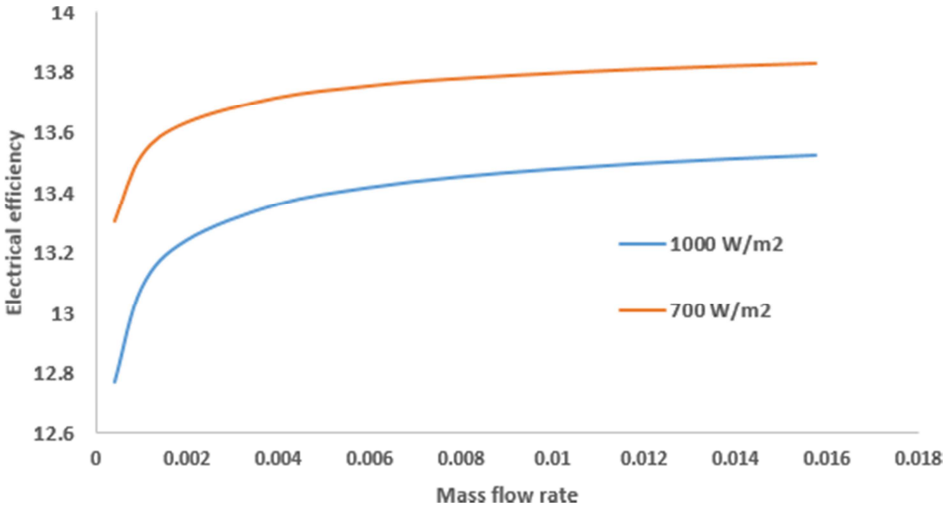

Figure 10. *Thermal efficiency for 700 W/m2 and 1000 W/m^2.*

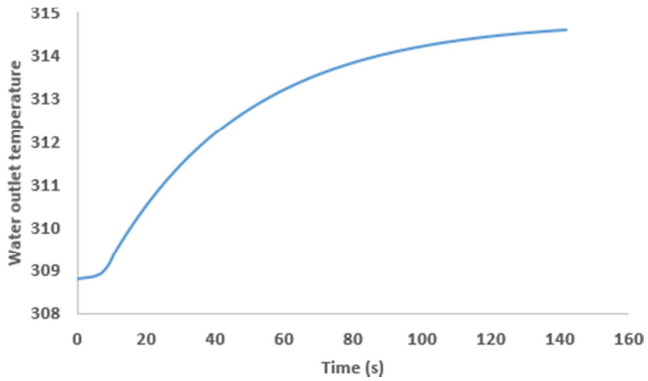

Figure 11. *Transient response of PVT system.*

As we examine the relationship between different factors, it becomes evident that both thermal and electrical efficiency exhibit an upward trend as the mass flow rate of water increases. However, an interesting counterpoint arises: while higher mass flow rates yield enhanced efficiency, they result in substantially lower water outlet temperatures. This has significant implications for applications requiring heated water, indicating that lower mass flow rates should be chosen in alignment with temperature needs. Illustrated in Figure 11, is the dynamic response of the PVT system as the mass flow rate is intentionally reduced from 0.002 kg/s to 0.001 kg/s. Notably, the transition to a steady state occurs rather swiftly, with the system stabilizing within a mere 2-3 minutes. This rapid response underscores the system's efficiency and adaptability in addressing changes in operational conditions.

5. Conclusion

This study focuses on a specific segment of a solar PVT system, specifically a single water pipe configuration. The mathematical modeling was conducted utilizing the

capabilities of the OpenFOAMv9 software package, while paraview facilitated the visualization of numerical outcomes. Through a meticulous comparison between numerical results and corresponding experimental data presented by Chow T, the study demonstrates the effective utility of the OpenFOAMv9 computational fluid dynamics (CFD) package in accurately simulating the investigated scenario. This work thus underscores the in-depth understanding and adept tuning achieved through this simulation approach. These insights not only advance optimization understanding but also offer a comprehensive groundwork for sound decision-making across diverse real-world solar energy implementations.

References

[1] A. and S. K. Suzuki, "Combined photovoltaic and thermal hybrid collector," *Japanese journal of applied physics 19, no. S2 (1980): 79.*

[2] S. G. B. K. B. Krishna R. Adhikari, "Solar Energy Potential in Nepal and Global Context," *Journal of the Institute of Engineering,* vol. Vol. 9, No. 1, pp. 95–106, 2014.

[3] J. J. Michael and S. Iniyan, "Performance of copper oxide/water nanofluid in a flat plate solar water heater under natural and forced circulations," *Energy Convers Manag*, vol. 95, pp. 160–169, May 2015, doi: 10.1016/J.ENCONMAN.2015.02.017.

[4] C. S. Rajoria, S. Agrawal, and G. N. Tiwari, "Exergetic and enviroeconomic analysis of novel hybrid PVT array," *Solar Energy*, vol. 88, pp. 110–119, Feb. 2013, doi: 10.1016/J.SOLENER.2012.11.018.

[5] T. T. Chow, "Performance analysis of photovoltaic-thermal collector by explicit dynamic model," *Solar Energy*, vol. 75, no. 2, pp. 143–152, Aug. 2003, doi: 10.1016/J.SOLENER.2003.07.001.

[6] H. G. Teo, P. S. Lee, and M. N. A. Hawlader, "An active cooling system for photovoltaic modules," *Appl Energy*, vol. 90, no. 1, pp. 309–315, Feb. 2012, doi: 10.1016/J.APENERGY.2011.01.017.

[7] O. Rejeb, H. Dhaou, and A. Jemni, "Parameters effect analysis of a photovoltaic thermal collector: Case study for climatic conditions of Monastir, Tunisia," *Energy Convers Manag*, vol. 89, pp. 409–419, Jan. 2015, doi: 10.1016/J.ENCONMAN.2014.10.018.

[8] A. A. B. Baloch, H. M. S. Bahaidarah, P. Gandhidasan, and F. A. Al-Sulaiman, "Experimental and numerical performance analysis of a converging channel heat exchanger for PV cooling," *Energy Convers Manag*, vol. 103, pp. 14–27, Oct. 2015, doi: 10.1016/J.ENCONMAN.2015.06.018.

[9] C. Good, "Environmental impact assessments of hybrid photovoltaic–thermal (PV/T) systems – A review," *Renewable and Sustainable Energy Reviews*, vol. 55, pp. 234–239, Mar. 2016, doi: 10.1016/J.RSER.2015.10.156.

[10] K. Sopian, H. T. Liu, S. Kakac, and T. N. Veziroglu, "Performance of a double pass photovoltaic thermal solar collector suitable for solar drying systems," *Energy Convers Manag*, vol. 41, no. 4, pp. 353–365, Mar. 2000, doi: 10.1016/S0196-8904(99)00115-6.

[11] R. C. Spijkerboer *et al.*, "Out of steam? A social science and humanities research agenda for geothermal energy," *Energy Res Soc Sci*, vol. 92, Oct. 2022, doi: 10.1016/j.erss.2022.102801.

[12] OpenFOAM, "OpenFOAM v7 User Guide," 2022.

[13] OpenFoam, "Paraview User's Guide," 2020.

[14] A. Khelifa, K. Touafek, H. Ben Moussa, I. Tabet, H. B. C. El Hocine, and H. Haloui, "Analysis of a Hybrid Solar Collector Photovoltaic Thermal (PVT)," *Energy Procedia*, vol. 74, pp. 835–843, Aug. 2015, doi: 10.1016/J.EGYPRO.2015.07.819.

[15] The open source CFD toolbox, "chtMultiRegionFoam: OpenFOAM: User Guide," *2021*.

[16] S. Misha, A. L. Abdullah, N. Tamaldin, M. A. M. Rosli, and F. A. Sachit, "Simulation CFD and experimental investigation of PVT water system under natural Malaysian weather conditions," *Energy Reports*, vol. 6, pp. 28–44, Dec. 2020, doi: 10.1016/J.EGYR.2019.11.162.

[17] S. Bensalem, M. Chegaar, and M. Aillerie, "Solar Cells Electrical Behavior under Thermal Gradient," *Energy Procedia*, vol. 36, pp. 1249–1254, Jan. 2013, doi: 10.1016/J.EGYPRO.2013.07.141.